NASA TECHNICAL NOTE

NASA TN D-4282

NASA TN D-4282

VISUAL OBSERVATIONS OF FLOW THROUGH A RADIAL-BLADED CENTRIFUGAL IMPELLER

by Richard F. Soltis and Max J. Miller

Lewis Research Center
Cleveland, Ohio

NATIONAL AERONAUTICS AND SPACE ADMINISTRATION • WASHINGTON, D. C. • JULY 1968

VISUAL OBSERVATIONS OF FLOW THROUGH A RADIAL-BLADED CENTRIFUGAL IMPELLER

By Richard F. Soltis and Max J. Miller

Lewis Research Center
Cleveland, Ohio

(Film supplement C-256 available on request)

NATIONAL AERONAUTICS AND SPACE ADMINISTRATION

For sale by the Clearinghouse for Federal Scientific and Technical Information
Springfield, Virginia 22151 – CFSTI price $3.00

VISUAL OBSERVATIONS OF FLOW THROUGH A RADIAL-BLADED CENTRIFUGAL IMPELLER

by Richard F. Soltis and Max J. Miller

Lewis Research Center

SUMMARY

A 7.44-inch- (18.89-cm-) diameter radial-bladed centrifugal impeller designed by the stream-filament technique was operated in water over a range of flow conditions. Flow through the blade passages was visualized by observing the movement of nylon tufts glued to the impeller and by injecting dye into the fluid at the pump inlet. Photographs and film sequences of the tufts and dye in the rotating passages are presented. A comparison of the visual observations is also made with the measured performance results and with the flow conditions within the blade passages as calculated from an analytical procedure.

INTRODUCTION

For some advanced rocket-engine systems, pumps requiring a variable thrust capability must maintain high levels of performance over a wide range of stable flow conditions. The ability to predict performance in the design of such pumping machinery requires a detailed knowledge of the internal flow mechanism within the passages of the pump over an extensive range of flow rates. Various methods have been used for investigating the internal flows of a rotating impeller for both compressible and incompressible flow conditions. For instance, references 1 to 3 discuss analytical methods that are used to obtain mathematical solutions to the equations governing the flows. However, necessary assumptions limit the ability of these methods to represent real flows. Other investigators have used detailed measurements taken as radial surveys located at both the inlet and the outlet of the impeller to make deductions of internal flow conditions. In some cases, actual internal flow measurements such as described in reference 4 have been used to determine flow conditions of impellers. However, these internal measurements

are extremely difficult to obtain and usually require large rotating machinery. Finally, flow visualization methods have been used whereby the investigator observes or views the actual flows within a rotating machine. In such cases, the rotor has been slowed by high-speed photography or by the use of a stroboscopic light.

Flow visualization studies using various techniques of combining variable-speed cameras with appropriate sources of light have proven extremely valuable for qualitative exploratory investigations and as a complement to the detailed flow measurements. In reference 5, the flow within a centrifugal pump impeller is visualized by inserting neutral-density globules into the water and photographing with a high-speed camera. Smoke injection in the passages of a centrifugal impeller has also been employed (ref. 6) to study flow oscillations, pulsatory separation, and various secondary-flow phenomena.

This report presents visual observations of the internal flow of a 7.44-inch- (18.89-cm-) diameter radial-bladed centrifugal pump impeller. This impeller was designed by the stream-filament technique of reference 1 and was tested in the cold-water, closed-loop tunnel at the Lewis Research Center. The flow observations are related to measurements taken with high-frequency-response transducers located at the inlet and the outlet of the impeller. The analytical procedure (ref. 1) was then used to determine flow conditions within the impeller, and the results were compared with the visual observations. Detailed steady-state measurements of the performance of this impeller are presented in reference 7.

The visual aids used in this investigation consist of nylon tufts attached to the rotor to indicate local directions of flow, black dye injected at the impeller inlet to illustrate flow distribution throughout the rotor, and finally, the occurrence of cavitation within the impeller to indicate areas of local pressure below vapor pressure. Throughout this report, flow conditions are presented in individual photographs or in a series of photographs (film strips) of the impeller flow passages. Since motion picture sequences give a more realistic presentation of actual flow conditions within a rotating impeller, a motion-picture supplement C-256 has been prepared and is available on loan. A request card and a description of the film are included at the back of this report.

SYMBOLS

H_{sv}	net positive suction head
N	speed
φ	flow coefficient
ψ	headrise coefficient

Subscript:

d design

Superscript:

$\bar{}$ mass averaged

APPARATUS AND PROCEDURE

A photograph of the impeller is presented in figure 1, and a detailed description is given in reference 7. The impeller has a total of 28 blades at the outlet: 7 main blades, 7 main splitter blades, and 14 small splitters. The outside diameter of the pump is 7.44 inches (18.89 cm). The portion of the flow path encompassed by two main blades is shown in figure 2, along with the channel identifications, denoted by the letters A to D. Nylon threads, or tufts, used for observing streamline flow patterns were distributed over the flow area of interest and were located as shown by the crosses in figure 2. Tufts were glued into drilled holes, and the glue was chipped away to provide a tuft hinge point as close to the metal surface as possible. There are 78 tufts throughout the four passages. The location of 15 tufts glued to the suction surface of one of the main blades is shown in figure 3.

For dye injection, a 1/4-inch- (0.635-cm-) outside-diameter stainless-steel probe with a 0.035-inch (0.089-cm) wall thickness was used. At the probe discharge, the inside diameter of the probe head was 0.062 inch (0.157 cm). A pipe pressure of 5 pounds per square inch (3.44×10^4 N/m^2) was suitable for dye injection. The dye was sent directly into the blade inlet close to the hub of the impeller.

The test facility is a closed-loop, cold-water tunnel. A schematic diagram indicating the location of the components of the test loop is shown in figure 4. A more detailed explanation of the test facility is given in reference 8. Some of the system capabilities include filtering the water to remove particles larger than 5 microns in diameter and deaerating the water to reduce the air content to less than 3 parts per million. All tests were made with water preconditioned in this manner.

The test procedure was to maintain the speed and inlet pressure constant and to vary the flow rate by means of a discharge throttle valve. This procedure was followed to define the overall performance of the pump that is reported in reference 7. In this report, only the performance at the highest inlet pressure is discussed. This performance is essentially the noncavitating type, although some cavitation appears at the highest flow coefficients. A 16-millimeter motion-picture camera was used which was capable of operating from 12 to 36 frames per second. The camera was synchronized to a stroboscopic light by means of a magnetic pickup on the rotor shaft. With the impeller rotating

at 3000 rpm, the framing rate of the camera was adjusted to 25 frames per second to allow observation of the same blade passage every second revolution. This technique was used for photographing the tufts. The type of film was Plus-X negative motion-picture film.

The second technique incorporated a high-speed camera and a continuous light source that consisted of two 750-watt floodlamps. The film type was Double-X panchromatic negative film. The camera operates with a rotating eight-sided prism and prints two pictures on each 16-millimeter frame. With this camera, as high as 16 000 pictures per second were obtained to give a partial time history of the flow through the impeller. This technique was used to slow down the motion of the dye within the blade passages.

Several positions of the camera and the light sources were tested in an effort to obtain a view of the maximum number of tufts with a minimum amount of glare from the plastic casing. Because of the thickness and curvature of the plastic casing and the high rate of curvature of the impeller hub section, focusing was critical. For the dye pictures, the glare from the window casing was not completely eliminated because the lights had to be placed only 2 inches (5 cm) away from the casing surface to obtain sufficient light for the high framing rates. This proximity of lights caused the plastic to heat very quickly and the field of view to become somewhat blurred. Thus, the dye pictures are not so clear as the tuft pictures.

Reference 7 discusses the instrumentation used in obtaining the measured performance of the impeller. For this investigation, high-frequency-response pressure transducers were also inserted at the pump inlet and outlet to measure pressure fluctuations over the flow range of the pump.

RESULTS AND DISCUSSION

Flow visualization can supplement the measured performance of a pump by providing qualitative information on the streamline flow paths and in particular, the flow directions. The best performance levels occur when the fluid streamlines are observed to flow smoothly and continuously throughout the blade passages. Any disruption of smooth streamline flow or failure of these streamlines to negotiate required passage curvature is usually reflected as a decrease in performance. It is, however, difficult to achieve a complete three-dimensional picture of the flow within a rotating impeller. Thus, techniques used to make the flow patterns more visible are generally applied to critical flow regions within the blade passages, and these results are then compiled to obtain a more complete flow picture.

For correlation with the visual studies, the measured performance characteristics of the impeller are shown in figure 5. The mass-averaged head-rise coefficient $\overline{\psi}$ is

shown as a function of the impeller-inlet averaged flow coefficient $\overline{\varphi}$ at a constant net positive suction head H_{sv}. A scale showing $\overline{\varphi}/\overline{\varphi}_d$ is also included on the abscissa. Data were obtained at an impeller rotative speed of 3000 rpm (97 ft/sec or 29.7 m/sec), and at a high level of net positive suction heat (192 ft or 58.5 m).

The curve of figure 5 represents measurements across the impeller alone and does not include any effects of flow through the scroll or diffuser section downstream of the impeller. The design flow coefficient for the impeller is 0.363. A discussion of the measured performance of this impeller is presented in reference 7. The impeller could be operated to a near-zero flow condition without sufficient evidence of facility vibrations or noise occurrence to cause suspension of operation.

Observations of Nylon Tufts

At most flow conditions, the tuft movements indicate some time variations of flow conditions when a number of frames are compared. The motion pictures clearly indicate the extent of these variations. However, single photographs cannot show variations of flow conditions. Thus, to provide a better presentation of average flow conditions, as well as the extent of variation of flow conditions, a sequence of photographs (film strips) is generally presented. Each individual photograph in the strip is taken two revolutions later than the preceding photograph. Thus, at the test speed of 3000 rpm, the time delay between frames is 1/25 second.

To facilitate the discussion and to identify more easily the tuft locations, the blade passages (fig. 6) are referred to by the letters A to D, and the frames are numbered 1 to 6, as depicted in the figures. Passage A is formed by the suction surface of a main blade and the pressure surface of a small splitter blade, whereas passage D is the passage formed by the pressure surface of a main blade and the suction surface of a small splitter. Because of the support that holds the plastic window in place, the first three rows (fig. 2) of tufts cannot be seen in the photographs. Also, part of channel A (fig. 6) is outside the field of view because of the necessary angle of the camera. Wherever applicable, comments of the tuft movement in this passage are included from the direct visual observations of the operator.

Photographs of the nylon tufts on the impeller hub are presented for a rotor speed N of 3000 rpm, an inlet pressure above vapor pressure H_{sv} of 194 feet, and the following flow conditions:

Flow coefficient, $\overline{\varphi}$	Design flow coefficient, $\overline{\varphi}/\overline{\varphi}_d$
0.602	1.66
.580	1.60
.532	1.46
[a].368	1.01
.220	.61
.170	.47
.075	.21

[a]Approximately design.

Near-design flow coefficient. - At a flow coefficient of 0.368 (fig. 6), which is close to the design flow coefficient (φ/φ_d = 1.01) the tufts indicate:

(1) Fluid streamlines that follow the blade directions reasonably well

(2) Small deviations of flow from the blade direction at the impeller outlet (tufts in row 7)

(3) No separated regions (suction surface tufts are steady all along blades)

(4) Reasonably steady flow, as indicated by small or negligible changes in tuft positions from frame to frame

(5) Nearly the same pattern of the tufts in all the passages, an indication of similar flow conditions in the four passages

Above-design flow coefficients. - As the flow is increased from the design value to a $\overline{\varphi}$ of 0.532 (fig. 7), no significant changes in the patterns of the tufts are noted; their pattern similarity from passage to passage denotes similar flow. Throughout the impeller, reasonably steady flows are believed to exist. However, some cavitation, which signifies a low-pressure region across the blades, occurs in the tip clearance region and extends into the blade passages. As the flow is increased (figs. 8 and 9), the cavitation extends further across the blade passages and increases in length along the blades. The cavitation shows the same general shape from blade to blade and remains relatively uniform from frame to frame. At these flow coefficients (figs. 8 and 9), a small sheet of surface cavitation can also be observed on the suction surface of the small splitters. The tuft pattern beneath the cavitation also appears nearly the same in all the frames.

Below-design flow coefficient. - When the flow is decreased from the design value to flow coefficients of 0.220 and lower (figs. 10 and 11), two significant changes in the tuft patterns are observed: noticeable changes in the tuft direction from frame to frame, which indicates increasing unsteadiness of flow, and varying tuft patterns from passage to passage, which indicates different amounts of fluid or flow rates in adjacent passages.

At $\overline{\varphi}$ equal to 0.220 (fig. 10), the following observations were made:

(1) In frame 1, passages B and D, the tufts are turned away from the pressure sur-

face to indicate the formation of a reverse flow region. In frames 4 and 5, however, the same tufts are turned toward the pressure surface to indicate unsteady flow conditions within the various passages.

(2) In passage D (frames 1 to 3), the direction of the tufts (row 4) near the suction surface of the blade suggests slight separation from the suction surface of the small splitter blade. The separation occurs in some periodic fashion as noted from frame to frame.

(3) The outlet tufts show that the deviation angle (difference between fluid angle and blade angle) at this flow coefficient is generally larger than the deviation angle at design flow.

At $\overline{\varphi}$ equal to 0.170 (fig. 11), where $\overline{\varphi}/\varphi_d$ is only 0.47, the following observations were made:

(1) All passages indicate that the flow is unsteady because each passage has a different flow pattern.

(2) Large flow reversals are indicated in passages A to C, and especially in frames 2 and 5.

(3) Most of the flow seems to be going through passage D, since, for the most part, the tufts in this passage are pointing downstream, especially along the pressure surface of the blade.

(4) Outlet tufts show irregular deviation angles. The operator noted that, at this flow coefficient, some flow was diverted from passage A to passage B. A closeup view taken at a slightly different camera angle (fig. 12) shows that the tufts at the inlet to passage A are turned away from the suction surface of the main blade toward passage B. Again, this turning was a periodic phenomenon.

At $\overline{\varphi}$ equal to 0.075 (fig. 13), where $\overline{\varphi}/\varphi_d$ is only 0.21, the following observations were made:

(1) The tufts in all passages exhibit large changes from their normal position to indicate a very unstable flow. (This instability is shown better in the motion-picture sequence.)

(2) The flow reversals are even larger than at $\overline{\varphi} = 0.170$ as shown by the number of tufts in all passages that indicate flow toward the blade inlet. The tufts remain in this position for a greater number of motion picture frames.

(3) Passage D again seems to be the passage carrying the most through flow, as indicated by the tufts turned toward the outlet in that passage.

At this flow coefficient ($\overline{\varphi} = 0.075$), the set of tufts on the suction surface of a main blade were also photographed (fig. 14). These tufts indicate separation at all radii in the blade leading-edge region. Separation is not as pronounced towards the trailing edge, especially along the hub of the blade. The operator noted that, at the low flows, these suction-surface tufts over the entire blade illustrated an unsteady condition by fluctuating back and forth in a seemingly random fashion.

Visual Observations of Dye

Black dye was injected into the pump at the blade inlet near the hub to make possible a comparison with the observations of the hub-mounted tufts. In general, the dye appeared to diffuse rapidly into the other stream tubes across the height of the blade. Thus, observations made from the flow during dye injection represent the flow distribution or travel of the flow front through the impeller.

Eight photographs of dye injection at a flow coefficient of 0.368 are presented in figure 15. Since the camera was operating at a speed of 16 000 pictures per second, this film strip of eight pictures depicts a total time of only 1/2000 second. Because the frames are somewhat distorted, the blade passages are identified by their relative position from the main blade in view. At $\varphi = 0.368$ and at all flows above $\overline{\varphi} = 0.220$, the channels were reasonably full and gave no evidence of separation or flow reversal. This observation agrees with those of the tuft pictures.

At a flow coefficient of 0.170 (fig. 16(a)), the flow appears to be separating from the main blade and the main splitter blade and flowing primarily through passages B and D, again in agreement with the tuft observations. When the flow is reduced to $\overline{\varphi} = 0.070$ (fig. 16(b)), small amounts of fluid seem to be flowing in a region close to the pressure surfaces of passages C and D. Passages A and B seem to receive little fluid. The motion-picture sequence of the dye injection better illustrates these flow conditions within the impeller. From this sequence, the flow is seen to exhibit a circulatory motion along with the through flow within a single blade passage. In the tuft sequences, however, this phenomenon was observed by the fluctuation of the tufts within the various passages.

Comparison with Measured Performance

The visually observed variations of flow conditions were compared in terms of the measured performance values. Figure 5 presented the mass-averaged head-rise coefficient as a function of the impeller-inlet averaged flow coefficient. Tufts at flow coefficients of 0.580, 0.532, and 0.368 indicate that the flow is passing smoothly through the impeller passages. Over this range of flow coefficients, the measured overall head-rise coefficient shows the negative slope generally associated with stable operation. At flow coefficients of 0.22 and lower, the tuft movements indicate an increased unsteadiness of flow, along with increasing amounts of separation from the suction surfaces, and eddy regions near the pressure surfaces. In this flow range, the measured head rise decreases from its maximum value.

In figure 17, the amplitude of peak-to-peak pressure measurements taken from high-frequency-response pressure transducers located at the pump inlet and outlet, respec-

tively, are noted on the pump performance curve. Over the flow range from 0.28 to 0.53, the measured peak-to-peak pressures at both the pump inlet and outlet were less than 4 pounds per square inch (2.76×10^4 N/m^2), which is approximately 3 percent of the total head rise across the impeller. No predominant frequencies were evident.

As the flow coefficient was increased from 0.532, the peak-to-peak amplitudes of the measured fluctuations increased slightly and consistently both at the impeller inlet and outlet measuring stations. At a flow coefficient near 0.600, the fundamental frequency of the main blades (350 cps or 350 Hz) became predominant at the pump inlet. This flow coefficient was one of the few operating points where a dominant frequency could be identified.

At a flow coefficient of 0.602, visual observations indicated that, in the vicinity of the diffuser tongue, a significant amount of cavitation was occurring within the impeller (fig. 18(a)). However, on the opposite side of the impeller housing (fig. 18(b)), a negligible amount of cavitation was observed within the blade passages to indicate that the degree of cavitation is not constant around the periphery of the impeller. This variance of cavitation results from the peripheral gradient of back pressure placed on the impeller as a result of the off-design flow around the scroll. It is not clear to what extent the cavitation and the peripheral gradient of impeller performance may be contributing to the fluctuating pressure measurements.

At flows below 0.28 (fig. 17), the magnitude of the pressure oscillations increases slightly again at both inlet and outlet to approximately 12 psi (82.7×10^3 N/m^2) at $\overline{\varphi} \approx 0$. The conditions revealed from visual observations in this flow range were an unsteady nature of the flow, nonuniformity of flow through the blade passages, and separation from the blade surfaces. No specific frequencies could be identified and no cavitation was observed. Thus, the pressure measurements and the visual observations complement each other and lead to similar conclusions concerning the variation of flow conditions.

Comparison with Analytical Procedures

Analytical procedures are used for predicting or studying flow conditions within the flow passages of centrifugal impellers. The validity of these analytical results is dependent, to a large extent, on the applicability of certain assumptions to reduce the complexity of a solution. Visual observations allow a preliminary evaluation of the applicability of analytical results to this impeller.

Two assumptions applied to the analytical procedure are that the flow is steady and that the flow is axisymmetric, that is, the same in all blade passages. Visual observations reveal that, for flow coefficients greater than approximately 0.22, the flow appears steady and the same in adjacent blade passages. However, the tufts cover just one-seventh of the circumferential extent of the impeller. Data measurements in reference 7

indicate that circumferential gradients of head rise occur above a flow coefficient value of approximately 0.3 and that the magnitude of the circumferential gradients (indicating asymmetry of flows) increases with the flow coefficient. At a $\overline{\varphi}$ of 0.22 (approximately 60 percent of the design flow) and lower, visual studies show increased degrees of unsteady flow and varying amounts of flow being directed into adjacent blade passages. Thus, for this configuration, the two assumptions of steady and axisymmetric flow approximate real flows at a reference flow, but these assumptions deviate increasing amounts as the flow is varied from the reference flow.

One interesting result obtained from the stream-filament analytical program (ref. 9) is the computation of zero or negative through-flow velocities. These velocities are interpreted as the occurrence of a reverse flow, or eddy region, and they are usually initiated on the hub near the pressure surface of the blade. At a selected reference flow rate, the eddies may be eliminated by controlling the passage flow area and/or curvature or by inserting splitter blades. Then, however, the eddy regions will usually be computed at some reduced flow from the reference value. The analytical program was modified to approximate the radial and circumferential growth of eddy regions over a range of flows.

The centrifugal impeller used in this investigation was designed to be free of eddies at the design flow coefficient of 0.363. At an operating point ($\overline{\varphi}$ = 0.368) very close to design flow, the visual observations indicate that no reverse flow regions exist near the blade pressure surface; thus, the program objective appears to have been attained.

Figure 19 shows sketches of the blades and of the approximate size and location of eddy regions on the hub surface as predicted by the analytical program for flow coefficients of 0.223 and 0.168. For comparison, the real flows on the hub surface, as indicated by the tufts, are shown in figure 20. The movement and positioning of the tufts away from the pressure surfaces indicate the occurrence of an eddy or reverse flow region. But the eddy regions do not seem to extend as far into the channel as the analytical results predict. In addition, the eddies do not form and remain static. Successive photographs indicated that the small separated regions form and then are swept downstream and then probably reform again. It was also shown that the flow patterns varied significantly in the four passages containing the tufts, as observed by the irregular tuft formations from passage to passage. These patterns indicate varying amounts of flow throughout the different passages.

At these lower flows, separation of flow from the blade suction surface (blade surface boundary-layer separation), as a result of high streamwise gradients of pressure, is also observed from the inlet tufts (fig. 20). Because of the boundary-layer development on the main blade, it is expected that greater separation would occur from the main blade and that the additional flow blockage due to this separation would tend to relieve the eddies occurring in the rest of the passage. The analytical program does not consider separation from this cause or account for its effect on the circumferential distributions of flow conditions.

CONCLUDING REMARKS

In the study of the complicated flow conditions throughout a centrifugal impeller, visual observations proved to be a useful supplement to measured data. They provide a picture of flow over the operating range, aid in the formulation of flow models used to analyze or predict flow conditions, and indicate regions of applicability of the flow models.

Flow patterns through the centrifugal impeller reported herein were made visible by means of nylon tufts fastened to the impeller passage surfaces and by the injection of dye into the flow stream. The results are qualitative and general to the extent that most centrifugal impellers would display the same trends of flow patterns over some range of operation.

The impeller was designed with the use of an analytical program for computing the flow conditions throughout impeller passages. Judicious positioning of splitter blades eliminated any calculated reverse flows in the region of the design flow coefficient of 0.363. Visual observations at design flow showed the fluid progressing smoothly through all flow passages with no evidence of separated flow. Thus, the design objective was evidently achieved.

At off-design flows, the visual observations were correlated with measured results and analytically predicted flow conditions. At flow coefficients above 0.53, a consistent increase in pressure fluctuations at the rotor inlet and outlet was measured. This increase correlated with the initiation and increase in the tip vortex cavitation in the impeller, as noted from visual studies. The visual observations also indicated that the cavitation was not symmetrical about the periphery of the impeller. This lack of symmetry probably results from the off-design flow in the volute, which generally imposes an asymmetric back pressure on the impeller.

At flow coefficients below 0.22, an increase in pressure fluctuations at the pump inlet and outlet was measured. The analytical results showed eddy or reverse flows in the hub-blade pressure surface region, extending along the complete flow path. The visual studies showed that the flow became increasingly unsteady as flow was reduced. Large, stationary eddy regions were not observed; rather, the direction of the tufts indicated that small eddy regions tended to form, be swept downstream, and then reform. Some periodic separation of the flow from the leading edge of the main blades and main splitter blades was observed. The result was that different amounts of flow were passing through adjacent blade passages. In this flow regime, analytical results, which currently do not account for boundary-layer effects (including separation) and which consider steady axisymmetric flow conditions, could not be expected to match real flow conditions. The results are too limited to associate the calculated eddy sizes with a generally unsteady flow condition.

In this report, the photographs presented are limited in number and do not completely convey the movement of the flow through the blade passages. A more graphic display of actual flow through the impeller is shown in the motion-picture supplement available on loan.

Lewis Research Center,
National Aeronautics and Space Administration,
Cleveland, Ohio, October 23, 1967,
128-31-06-28-22.

REFERENCES

1. Hamrick, Joseph T.; Ginsburg, Ambrose; and Osborn, Walter, M.: Method of Analysis for Compressible Flow Through Mixed-Flow Centrifugal Impellers of Arbitrary Design. NACA Rep. 1082, 1952.

2. Ellis, Gaylord O.; and Stanitz, John D.: Comparison of Two- and Three-Dimensional Potential-Flow Solutions in a Rotating Impeller Passage. NACA TN 2806, 1952.

3. Wu, Chung-Hau: A General Theory of Three-Dimensional Flow in Subsonic and Supersonic Turbomachines of Axial-, Radial-, and Mixed-Flow Types. NACA TN 2604, 1952.

4. Michel, Donald J.; Ginsburg, Ambrose; and Mizisin, John: Experimental Investigation of Flow in the Rotating Passages of a 48-Inch Impeller at Low Tip Speeds. NACA RM E51D20, 1951.

5. Boyce, M. P.: A Practical Three-Dimensional Flow Visualization Approach to the Complex Flow Characteristics in a Centrifugal Impeller. Paper No. 66-GT-83, ASME, Mar. 1966.

6. Maillet, E.; and LeManach, J.: Visualization of Incompressible Flow in the Passage of a Centrifugal Impeller. Rep. No. TIL/T4825, Ministry of Supply, Great Britain, 1957.

7. Miller, Max J.; and Soltis, Richard F.: Detailed Performance of a Radial-Bladed Centrifugal Pump Impeller in Water. NASA Technical Note, estimated publication date, Jan. 1968.

8. Soltis, Richard F.; Anderson, Douglas A.; and Sandercock, Donald M.: Investigation of the Performance of a 78° Flat-Plate Helical Inducer. NASA TN D-1170, 1962.

9. Stockman, Norbert O., and Kramer, John L.: Method for Design of Pump Impellers Using a High-Speed Digital Computer. NASA TN D-1562, 1963.

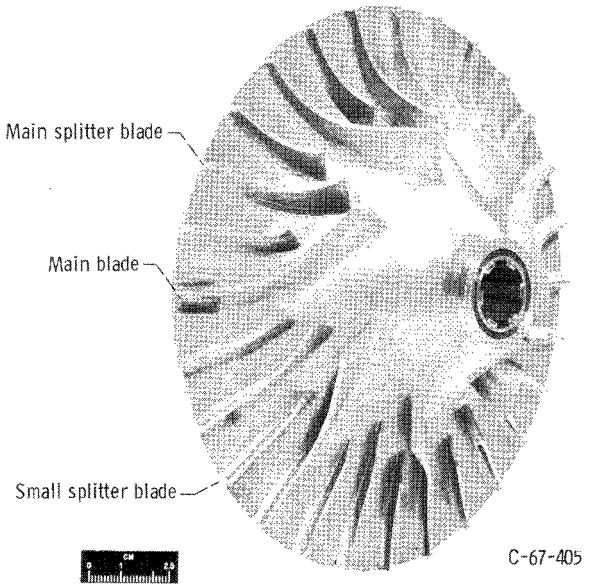

Figure 1. - Test rotor.

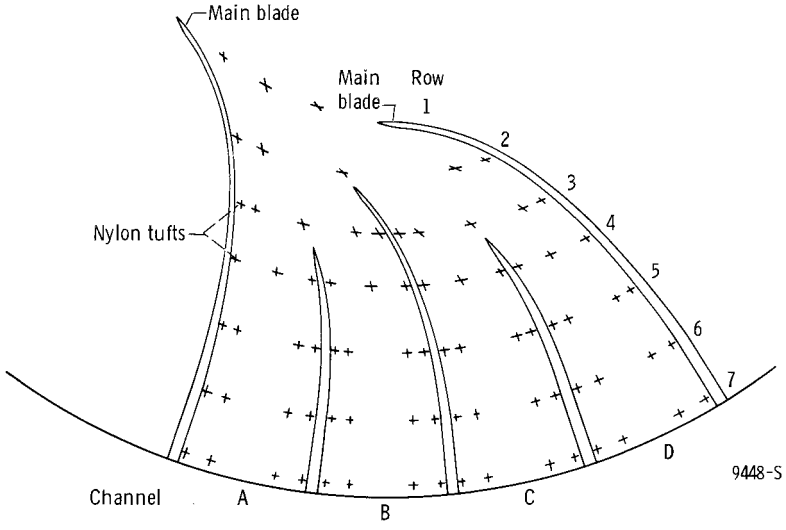

Figure 2. - Schematic diagram showing location of 78 tufts attached to hub of impeller.

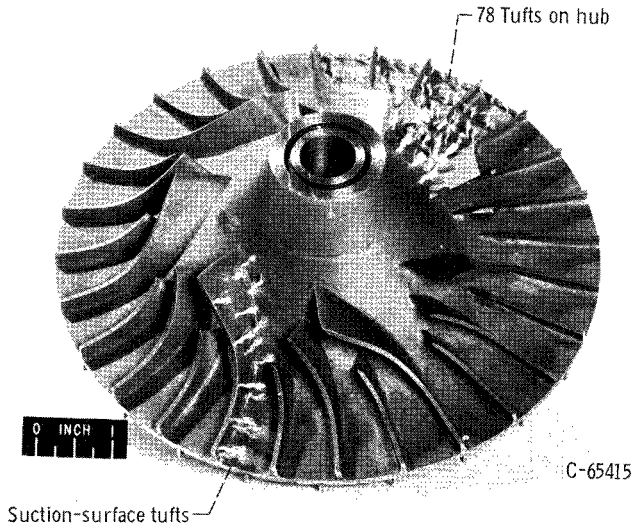

Figure 3. - Impeller with attached tufts.

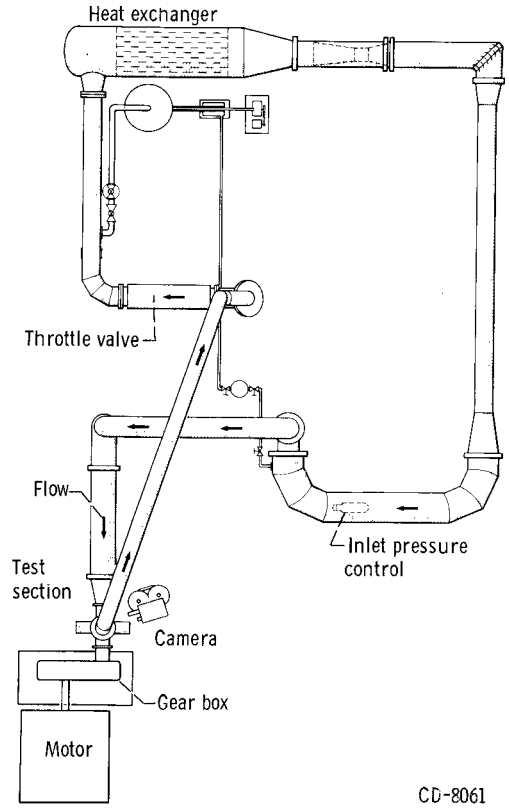

Figure 4. - Test facility and location of test loop components.

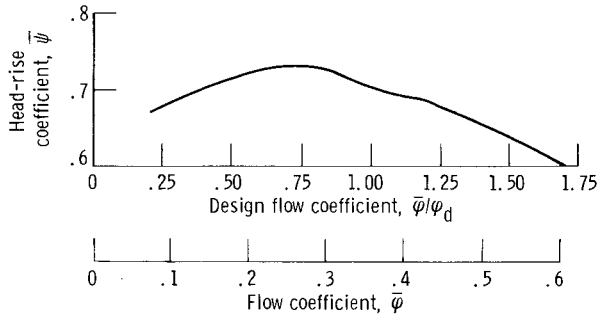

Figure 5. - Overall performance for high (70 psig or 482.3x10^3 N/m^2) inlet pressure conditions. Impeller outlet tip speed, 97.3 feet per second (29.67 m/sec).

Frame

1

2

3

4

5

6

Figure 6. - Film sequence showing positioning of tufts at near-design flow coefficient of 0.368.

Frame

1

2

3

4

5

6

Figure 7. - Film sequence showing positioning of tufts at above-design flow coefficient of 0.532.

Figure 8. - Film sequence showing positioning of tufts at above-design flow coefficient of 0.580.

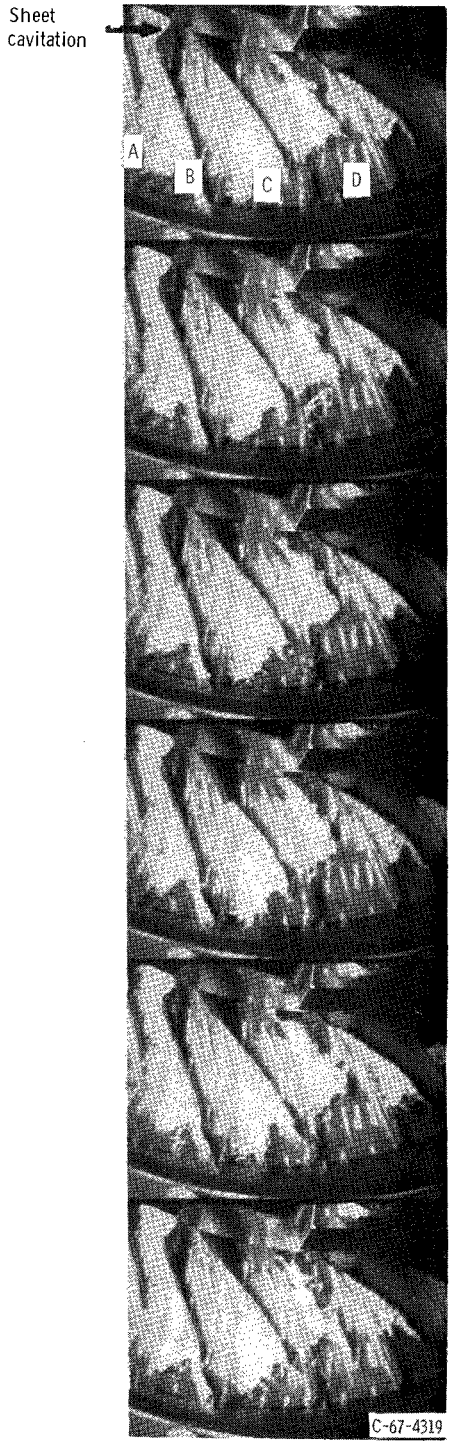

Figure 9. - Film sequence showing positioning of tufts at above-design flow coefficient of 0.602.

Frame

1

2

3

4

5

6

Figure 10. - Film sequence showing behavior of tufts at below-design flow coefficient of 0.220.

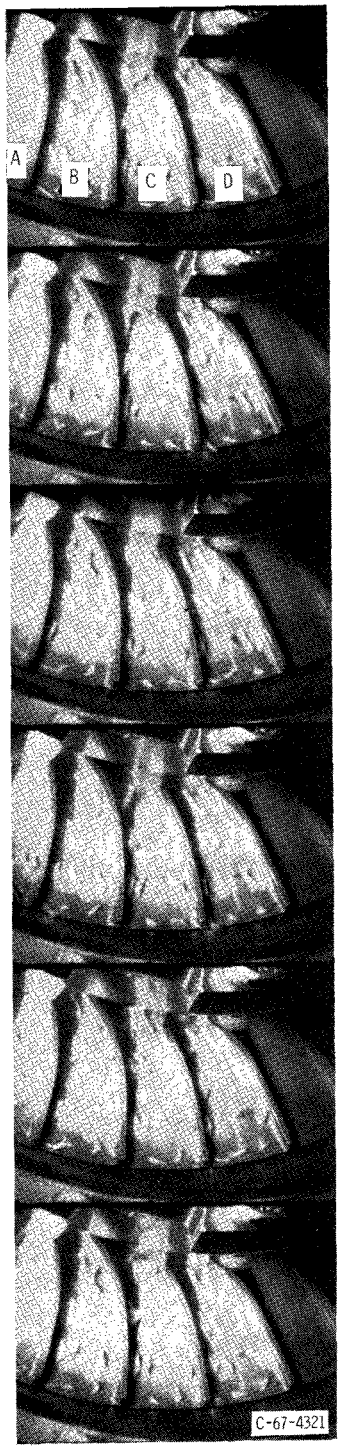

Frame

1

2

3

4

5

6

Figure 11. - Film sequence showing behavior of tufts at below-design flow coefficient of 0.170.

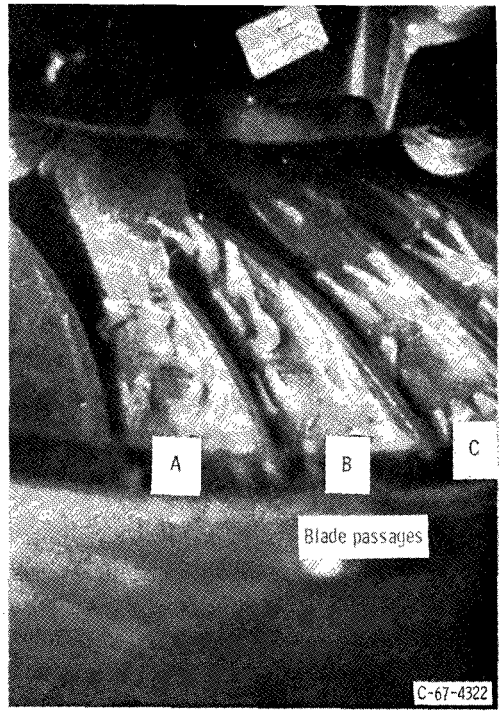

Figure 12. - Closeup view of tufts in blade-inlet region at flow coefficient of 0.170.

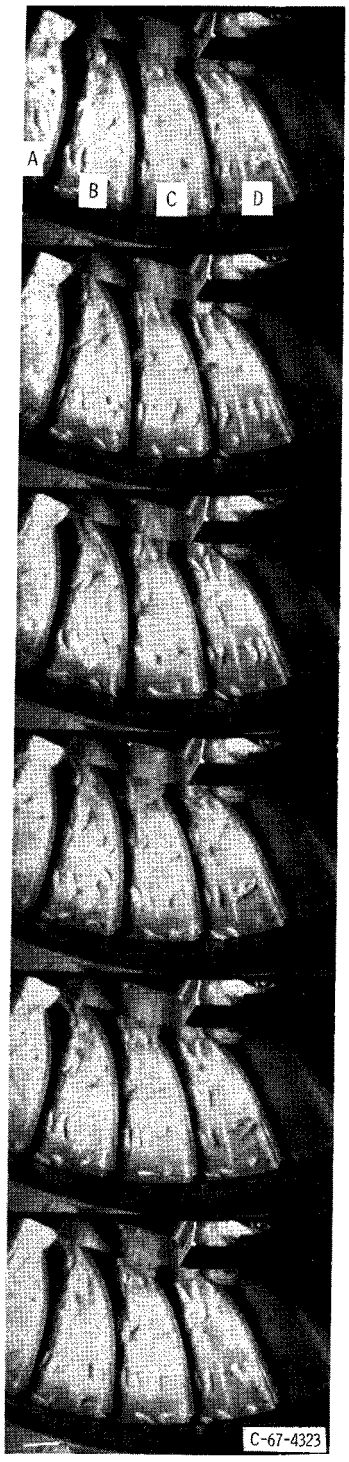

Figure 13. - Film sequence showing behavior of tufts at below-design flow coefficient of 0.075.

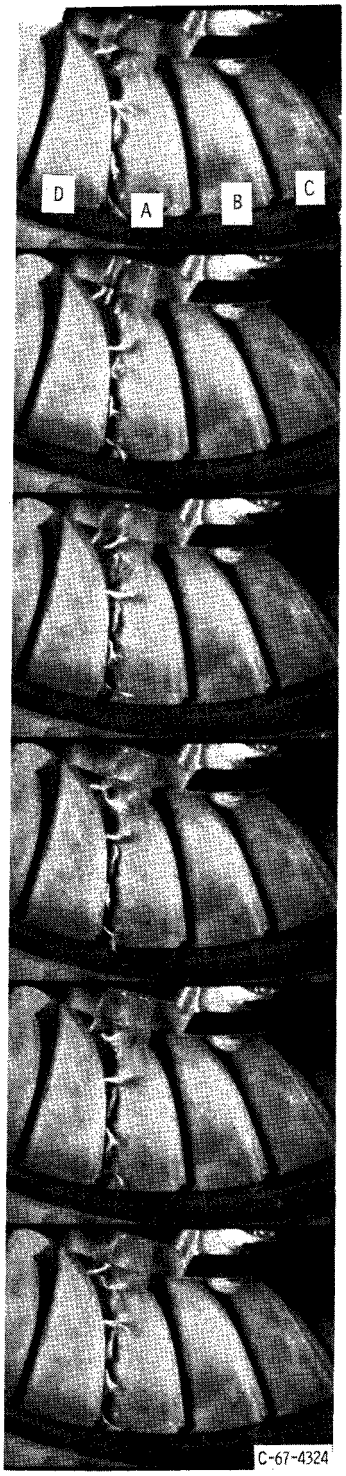

Figure 14. - Film sequence showing positioning of tufts on blade suction surface at low flow coefficient of 0.075.

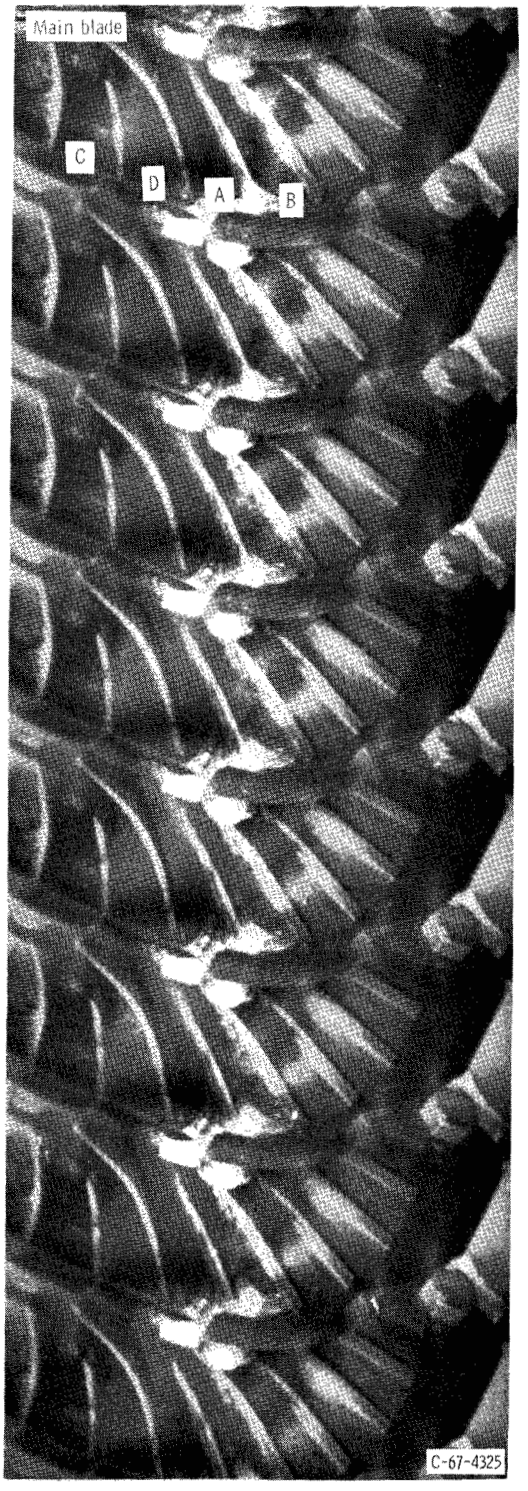

Frame

1

2

3

4

5

6

7

8

Figure 15. - Film sequence showing dye in blade passages at near-design flow coefficient of 0.368.

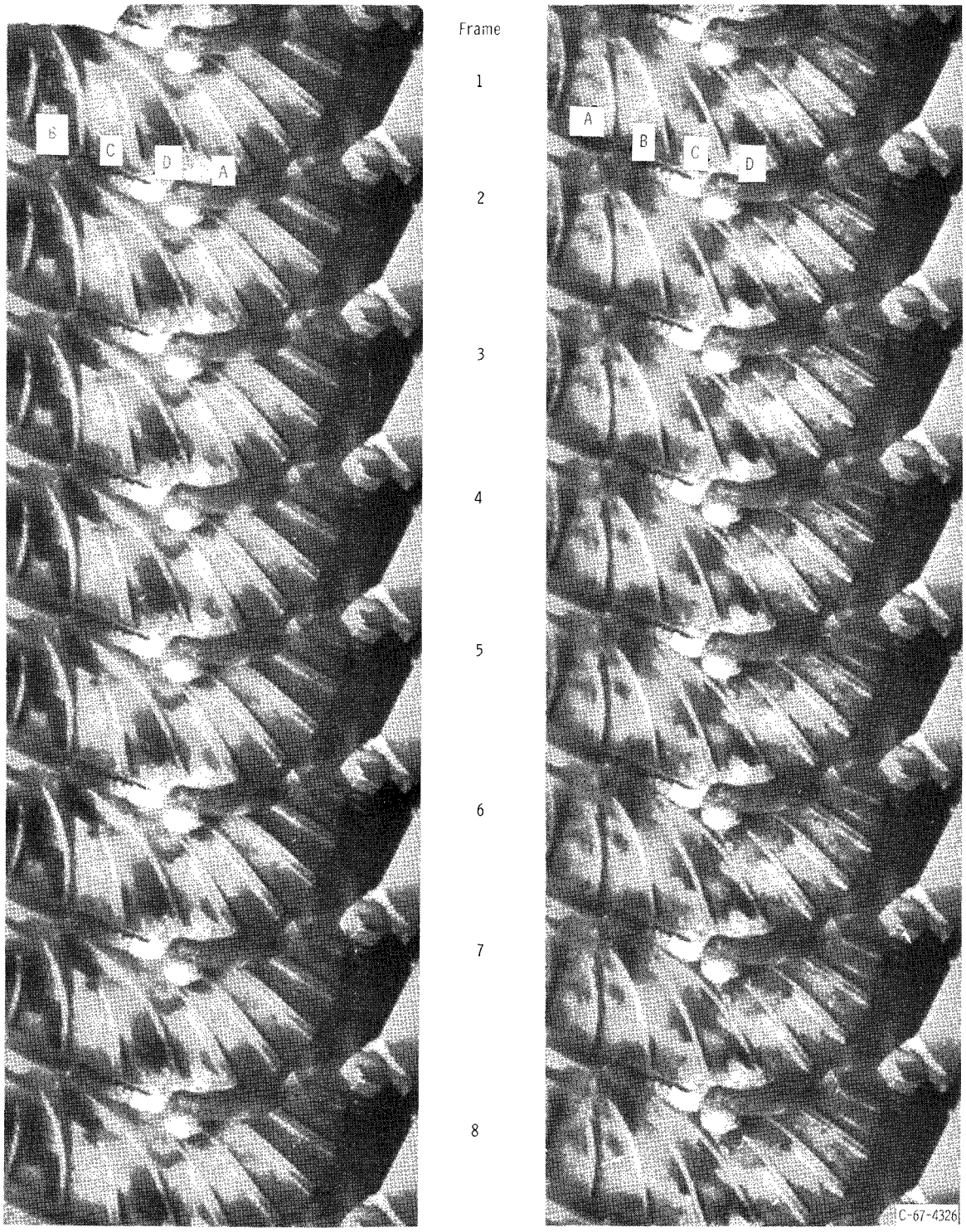

(a) Below-design flow coefficient, 0.170.

(b) Below-design flow coefficient, 0.075.

Figure 16. - Film sequence showing dye in blade passages.

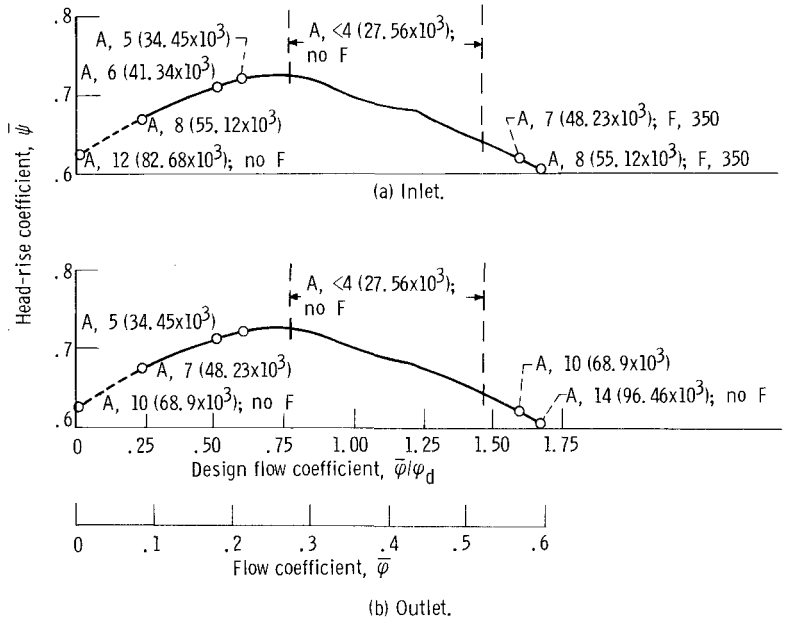

Figure 17. - Pump performance characteristics indicating magnitude and frequency of pressure fluctuations measured from high-frequency-response pressure transducers. Amplitude A is given in psi (N/m^2) and frequency F is given in cycles per second or hertz.

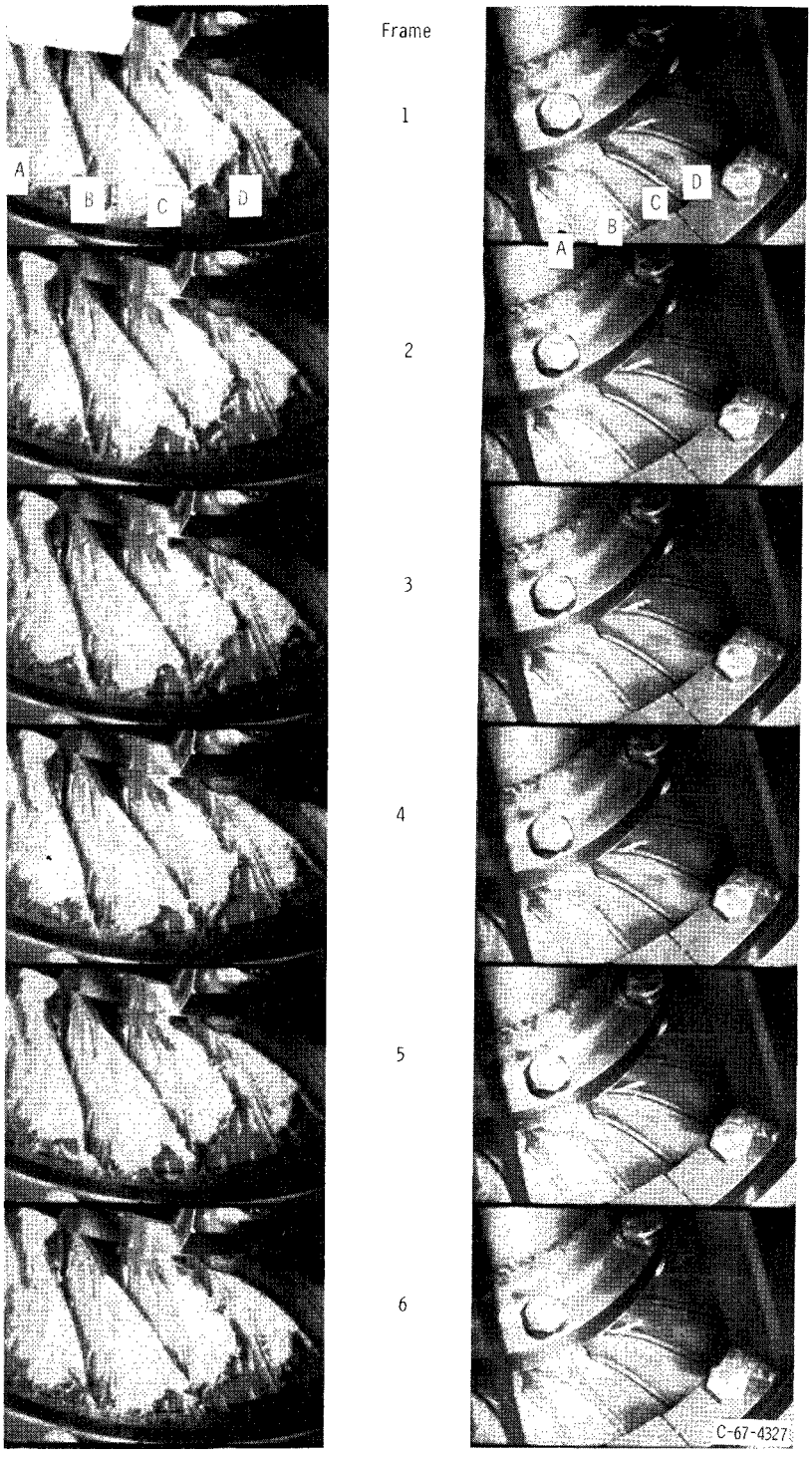

(a) In diffuser tongue region.

(b) At 180° from diffuser tongue.

Figure 18. - Film sequence showing cavitation within impeller at high flow coefficient of 0.602.

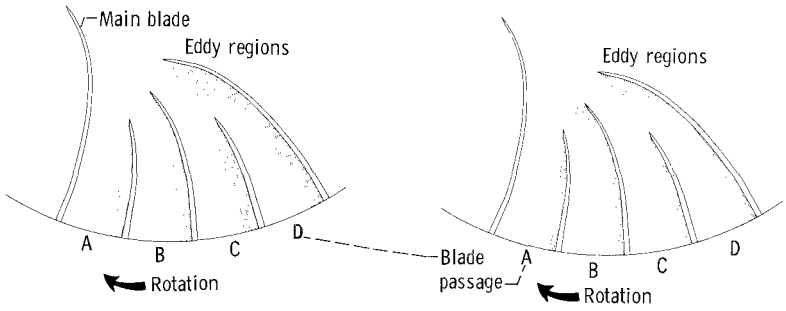

(a) Flow coefficient, 0.168. (b) Flow coefficient, 0.223.

Figure 19. - Schematic diagram showing location and size of eddy regions on impeller hub as computed from analytical procedure.

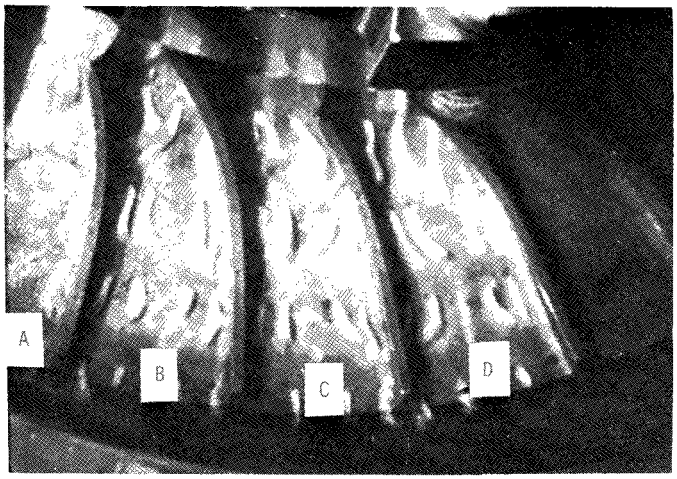

(a) Flow coefficient, 0.176.

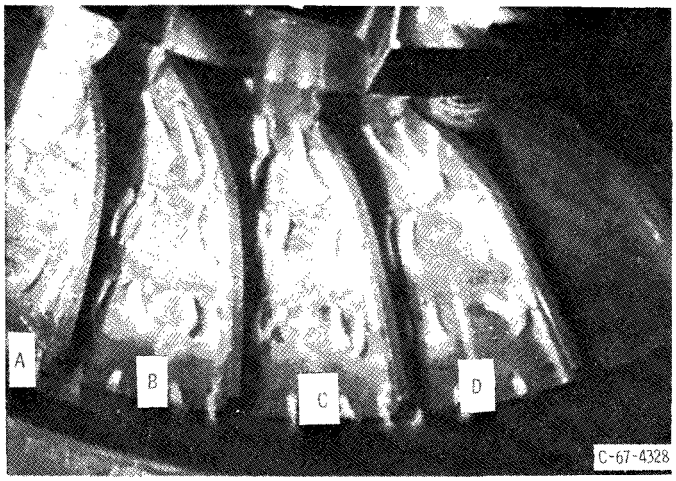

(b) Flow coefficient, 0.220.

Figure 20. - Closeup of tuft positions at low flows.

Motion-picture film supplement C-256 is available on loan. Requests will be filled in the order received. You will notified of the approximate date scheduled.

The film (16 mm, 16 min, color, sound) shows flow conditions through the passages of a radial-bladed centrifugal pump impeller operated in water which are examined over a wide range of flow rates. Visualization of the flow is made possible by the use of nylon tufts glued to the impeller surfaces and by the injection of black dye into the flow at the impeller inlet. A comparison is made between the visual observations and the measured performance results.

Film supplement C-256 is available on request to:

Chief, Technical Information Division (5-5)
National Aeronautics and Space Administration
Lewis Research Center
21000 Brookpark Road
Cleveland, Ohio 44135

CUT

Date

Please send, on loan, copy of film supplement C-256 to
TN D-4282

Name of Organization

Street Number

City and State Zip Code

Attention: Mr.
Title

NATIONAL AERONAUTICS AND SPACE ADMINISTRATION
WASHINGTON, D. C. 20546
OFFICIAL BUSINESS

FIRST CLASS MAIL

POSTAGE AND FEES PAID
NATIONAL AERONAUTICS AND
SPACE ADMINISTRATION

"The aeronautical and space activities of the United States shall be conducted so as to contribute . . . to the expansion of human knowledge of phenomena in the atmosphere and space. The Administration shall provide for the widest practicable and appropriate dissemination of information concerning its activities and the results thereof."

—NATIONAL AERONAUTICS AND SPACE ACT OF 1958

NASA SCIENTIFIC AND TECHNICAL PUBLICATIONS

TECHNICAL REPORTS: Scientific and technical information considered important, complete, and a lasting contribution to existing knowledge.

TECHNICAL NOTES: Information less broad in scope but nevertheless of importance as a contribution to existing knowledge.

TECHNICAL MEMORANDUMS: Information receiving limited distribution because of preliminary data, security classification, or other reasons.

CONTRACTOR REPORTS: Scientific and technical information generated under a NASA contract or grant and considered an important contribution to existing knowledge.

TECHNICAL TRANSLATIONS: Information published in a foreign language considered to merit NASA distribution in English.

SPECIAL PUBLICATIONS: Information derived from or of value to NASA activities. Publications include conference proceedings, monographs, data compilations, handbooks, sourcebooks, and special bibliographies.

TECHNOLOGY UTILIZATION PUBLICATIONS: Information on technology used by NASA that may be of particular interest in commercial and other non-aerospace applications. Publications include Tech Briefs, Technology Utilization Reports and Notes, and Technology Surveys.

Details on the availability of these publications may be obtained from:

SCIENTIFIC AND TECHNICAL INFORMATION DIVISION

NATIONAL AERONAUTICS AND SPACE ADMINISTRATION

Washington, D.C. 20546